Int. J. Solids Structures Vol. 21, No. 3, pp. 245–266, 1985
Printed in the U.S.A.

0020–7683/85 $3.00 + .00

PETALLING OF THIN, METALLIC PLATES DURING PENETRATION BY CYLINDRO-CONICAL PROJECTILES

B. LANDKOF† AND W. GOLDSMITH
Department of Mechanical Engineering, University of California, Berkeley, CA, U.S.A.

(*Received* 25 *July* 1983)

Abstract—A theoretical and experimental investigation has been undertaken to study the processes of perforation at normal incidence of thin, soft aluminum plates by hard-steel cylindro-conical projectiles of 30° half-cone angle. The analysis is executed by means of an energy balance for a rigid/perfectly-plastic or work-hardening material. For an intact plate, where petalling always occurs, consecutive stages of the process involve initial crack propagation followed by plastic hinge motion out to the position of crack arrest, followed by petal bending due to hinge rotation up to and beyond the point of projectile passage. In the case of central impact on an initial hole in the plate, the first stage constitutes an enlargement of the hole, followed by crack propagation and bending of trapezoidal regions of the plate until the projectile has either perforated or is embedded in the target.

Tests conducted on 2024-0 aluminum with a thickness of 3.175 mm indicated a condition so that if the initial hole radius was greater than about ¾ that of the 12.7 mm diameter hard-steel projectile, cracking did not occur and all the energy was absorbed by hole enlargement. Furthermore, for each initial impact velocity, an optimal hole radius was found to exist where a maximum energy absorption of the plate occurred, greater than for the intact target. This phenomenon was qualitatively substantiated by the theory; discrepancies in magnitudes are attributed to the neglect of certain energies in the analysis, particularly that of dishing. Excellent correlation was found between the theoretical prediction for the terminal velocity of a projectile striking the intact plate and test results when an estimate of the dishing energy for the plate was included.

LIST OF SYMBOLS

a	crack length
A	area of crack
b	constant
B	base width of petal
B_0	width of petal at tip
C	variable of integration
E	Young's modulus
$F(n)$	petal function
G	energy per unit crack area for crack extension
G_c	unit surface area for extended crack
h	plate thickness
h'	average crater thickness after hole enlargement
I	moment of inertia
k, k_1, k_2	mass ratio parameters
K_I	stress intensity factors for Mode I cracks
l	length of crack or cantilever beam
m	projectile mass
M	bending moment
M^*	maximum moment
n	number of petals
r	radial coordinate or distance
R	hole or crater radius
R_B	projectile radius
v	striker velocity
V	volume
w	transverse displacement
W	total energy
x	travel distance of plastic hinge
y	local petal width
Y	yield stress
α	half-cone angle of striker
γ	work-hardening parameter
ϵ	strain

† Current address: Box 2250, Haifa, Israel.

Θ petal rotation angle
λ any distance from petal base less than x
μ cantilever petal mass
ν Poisson's ratio
ρ mass density of target
σ stress
ω angular velocity

Subscripts

c crack
C central
d dynamic
D distal side at end of plastic hole enlargement
e equivalent
E end of plastic hole enlargement and onset of cracking
f final
F fracture
i initial
k kinetic
n normal
o original
p plastic
r radial
R rotational
t total
T tangential
z axial
1 at end of Stage 1 for intact plate (crack arrest)
2 at end of Stage 2 for intact plate (projectile perforation)
50 ballistic limit
θ circumferential

INTRODUCTION

During the last few decades, the phenomenon of petalling during penetration of thin plates by conically-headed cylindrical projectiles has been studied extensively. Experimental and analytical efforts have been directed towards finding the amount of energy absorbed in this penetration mode. Analytical models capable of correctly predicting this energy will have substantial practical value in predicting the terminal projectile velocity or a ballistic limit for a given impact configuration. The energy approach was utilized in previous investigations by Bethe [1], Taylor [2], Thomson [3] and, more recently, Johnson [4].

The solutions utilized in these investigations assumed formation of a crater and calculated the plastic energy required for its construction. The approach was primarily of a static nature with the exception of [4] where some dynamic effects were included. The crater was assumed to conform to the configuration of the projectile throughout the entire penetration process.

Based on experimental evidence, the present investigation proposes a new direction for the analysis of the penetration of thin, metallic plates by cylindro-conical strikers at normal incidence. The method will take into account the petalling of the plate and a radial crack propagation process. The bending of the petals during the penetration process will be modeled using the method of plastic hinges, permitting the evaluation of the energy absorbed during this stage. The analysis includes inertial effects.

In order to calculate the total amount of energy absorbed by the plate during petalling, all phenomena occurring during the event should be taken into account. In several previous investigations [3, 5] it has been shown that the amount of energy dissipated by heat (friction) in the perforation process can be neglected compared to the plastic work. It will be demonstrated in the sequel that the amount of energy needed for extension of radial cracks is small and may be neglected at high impact velocities relative to the ballistic limit. Thus, the principal source of energy consumption is the plastic deformation of the target. This process involves two types of plastic work: that required for petal bending and that used for plate dishing. These deformations are sketched in Fig. 1.

This paper will deal primarily with petalling: an exact determination of the energy

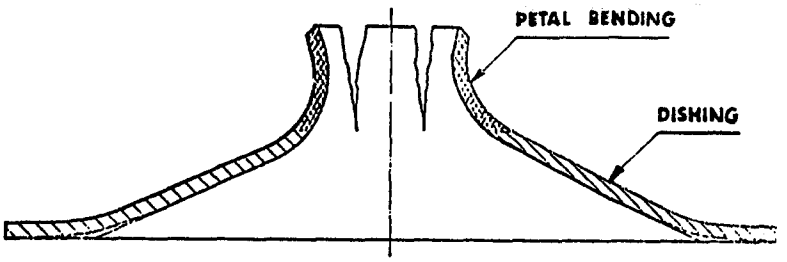

Fig. 1. Plate perforation by a conically-tipped projectile showing petal formation, bending and dishing.

of plate dishing, a major effort, will be the subject of a future investigation. An approximation for the dishing energy for the intact plate is provided from a previous investigation [6] which accounts only for the plastic work due to radial stretching and is based on an observed exponential terminal plate profile. While crucial near the ballistic limit, the amount of this dishing energy for initial projectile speeds well above this limit is relatively small. Thus, the present analysis without consideration of bending should be a good approximation of the actual event in the higher velocity domain. The investigation deals with circular thin metallic plates of a strain-rate independent material. Impact velocities in the subordinance range (90–460 m/s) or ordinance range (460–920 m/s) were employed.

The projectile is cylindrical with a 60° conical nose, made of hard steel and assumed in the analysis as a rigid, nondeformable body. The plate is regarded as thin, which implies that stress and deformation gradients do not exist in the target thickness direction.

In the sequel, the influence of an initial hole on the perforation process for a symmetric normal impact is also discussed. The investigation concentrated on experimental aspects of the event, leading to a proposed qualitative explanation. Further analytical work must be executed to calculate accurately the energy transferred to the plate for the case of such an initial circular hole during the penetration process. Experimentally, it was found that an optimal size of hole exists for which the energy absorption in the plate is maximal and substantially greater than for an intact plate. An explanation of this phenomenon is proposed.

CRACK PROPAGATION DURING THE PROCESS OF PETALLING FOR NORMAL IMPACT OF CYLINDRO-CONICAL PROJECTILES

The beginning of the petalling process during perforation is always associated with fracture initiation. Experiments were performed to establish the sequence of events during crack initiation and propagation. Figure 2 shows that immediately after initial contact by the projectile nose, a star-shaped crack is formed, involving negligible energy transfer; its fissures subsequently propagate outwards under the pressure of the moving projectile. After partial perforation, the moving nose of the projectile tends to enlarge the circumference of the initiated hole, as shown in Fig. 3. The hoop stress is thus responsible for further radial extension of the cracks.

This damage pattern, sketched in Fig. 4, is clearly a Mode I type of crack propagation. The amount of energy that is spent to extend the star-shaped crack will now be calculated.

According to Griffith's postulate, the amount of energy per unit crack area needed for extension of the crack, G, must be greater than the unit surface energy of the extended crack, G_c, so that $G > G_c$ for the radial crack growth. For the first mode, G is given by

$$G = \frac{K_I^2}{E} \tag{1}$$

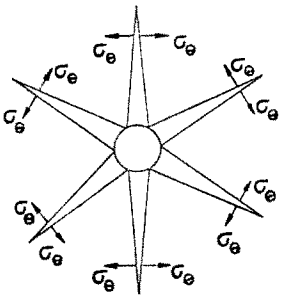

Fig. 4. Star crack pattern with 6 petals produced by circumferential stresses.

where K_I is the stress intensity factor for Mode I and E is the static modulus of elasticity. K_I can be approximated by the solution found by Westmann [8] for a linear star-shaped crack of any number of petals, as shown in Fig. 4:

$$K_I = \sigma\sqrt{\pi a}F(n). \tag{2}$$

$F(n)$ is a function of petal number n as indicated in Fig. 5 for a symmetrical pattern, and σ is the stress and a the length of the crack as shown.

Substituting eqn (2) into eqn (1) yields

$$G = \frac{\pi a\sigma^2 F^2(n)}{E}. \tag{3}$$

In order to obtain the total energy, eqn (3) must be multiplied by the total area of cracks $A_t = 2nh_0a$

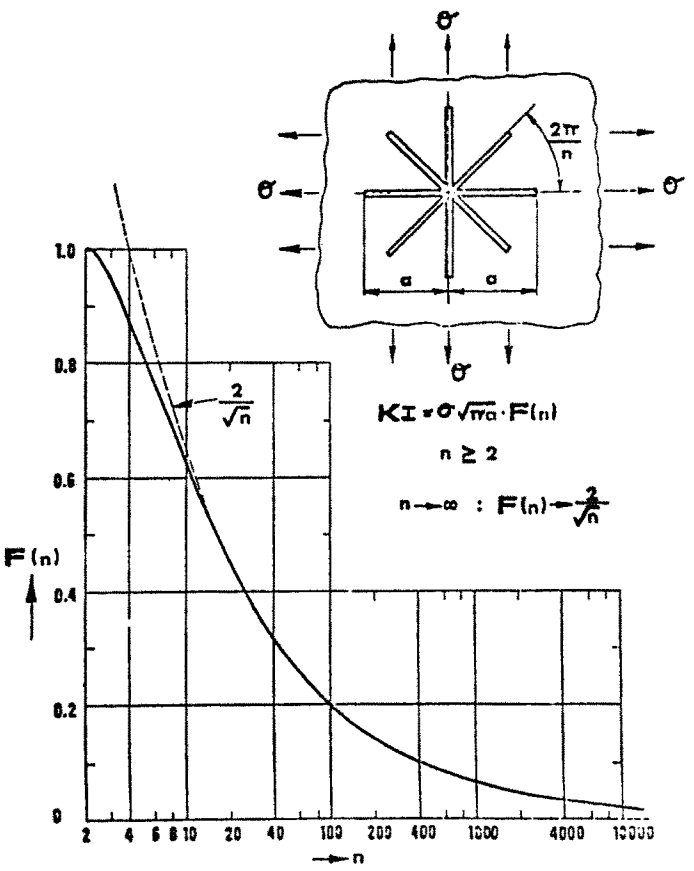

Fig. 5. Petal function $F(n)$ in terms of the number of petals n for a symmetrical crack pattern.

Fig. 2. Initial formation of a star-shaped crack.

Fig. 3. Terminal configuration of the petals bent after formation of a star-shaped crack.

$$W_c = GA_t = \frac{2\pi\sigma^2 h_0 a^2 n F^2}{E} . \tag{4}$$

Finally, it will be assumed that $\sigma = Y$ in order to determine an upper bound for this energy

$$W_c = \frac{2\pi n h_0}{E} [aYF(n)]^2 \tag{5}$$

where Y = yield stress in tension and
h_0 = initial thickness of the target plate.

Later, it will be shown that this energy is small compared to the plastic work of petal and plate bending.

ENERGY ABSORBED IN PETAL BENDING DUE TO ACTION OF PLASTIC HINGES

As shown in Figs. 2 and 3, petal formation results from the bending of triangular plate sections formed by the outward crack propagation due to the pressure of the conical nose. The analysis of this process requires the following assumptions:

(a) The force exerted by the moving conical nose of the projectile, of mass m, is always applied at the tip of the petal in the direction normal to the plate.
(b) Geometrical effects due to large deformations are neglected, i.e. the analysis is linear.
(c) The material is regarded as rigid, ideally plastic, so that no deformation occurs when the bending moment at a petal cross-section is smaller than the plastic moment M_p and indefinite deformation can occur when it exceeds M_p.
(d) Only projectile impacts are considered in which the initial kinetic energy ($\frac{1}{2} mv_i^2$) is much larger than the maximum elastic energy that the target plate can absorb. Hence, only plastic work is taken into account in the energy balance.
(e) The speed of crack propagation is assumed to be always higher than the plastic hinge velocity.

Since the petals are initiated at the moment of impact and grow in length l with outward propagation of the star crack, it may be assumed that at each stage of projectile motion, one deals with a cantilever beam of constant thickness and triangular shape. The fixed end of this beam moves outwards with the expansion of the star crack. The situation is described by Fig. 6.

There are two stages in the absorption process: During the outward crack propagation, there will be parallel outward motion of the plastic hinges in the petals until the cracks are arrested and the hinges arrive subsequently at this "built-in" end (the root of the petal), Fig. 7. The petals experience a rotation Θ_t during and at the end of this phase. After the first stage, the moving projectile and the petals still possess kinetic energy; therefore, additional motion will take place. This time, the plastic hinge is fixed at the root of the petal and a rigid rotation of the petal about its root by an angle Θ_s occurs, of a magnitude sufficient to ensure free passage of the projectile. At the end

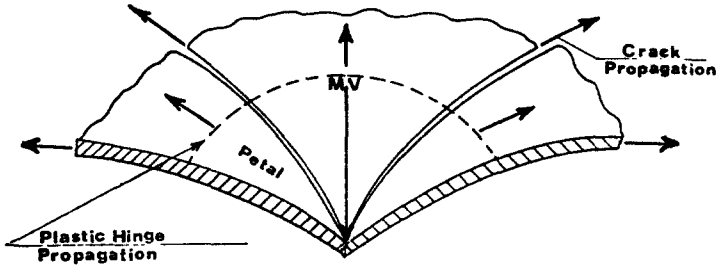

Fig. 6. Propagation of the cracks and plastic hinge.

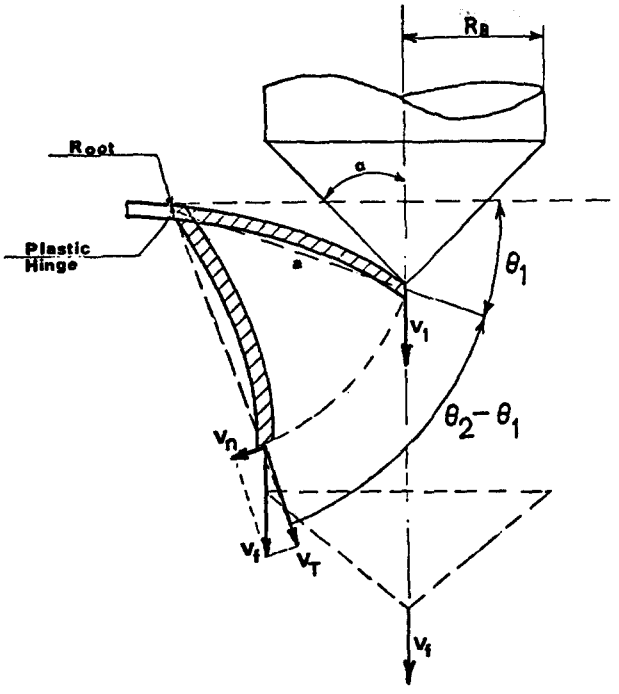

Fig. 7. Arrival of plastic hinges at the root of the petal.

of this second stage the petals still may have some residual kinetic energy, especially in the case of thin plates. In this event, the total petal rotation will exceed angle Θ_2 as shown in Fig. 8 and observed in the tests.

The energy absorbed in the first stage of deformation will now be calculated. This problem was solved by Parkes [9] and its adaptation to a triangular cantilever beam is presented by Johnson [10]. This approach will be closely followed here.

The plastic moment for a cantilever beam of constant thickness h_0 and length l is given by

$$M_p = Y\frac{Bh_0^2}{4}\frac{x}{l} \tag{6}$$

where x is the distance of travel of the plastic hinge after time t and λ is any distance from the tip of the petal such that $\lambda < x$. All other parameters are defined in Fig. 9. The width of the petal with base width B at a distance x from the tip is

$$b = \frac{Bx}{l}. \tag{7}$$

It is assumed that n petals are formed. Each petal is struck at the tip by a mass equal

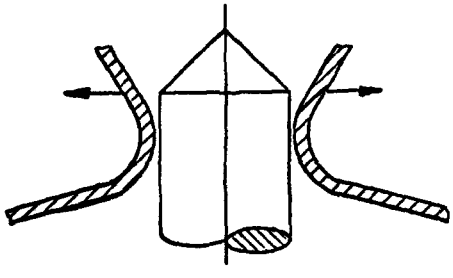

Fig. 8. Additional outward petal motion due to residual kinetic energy.

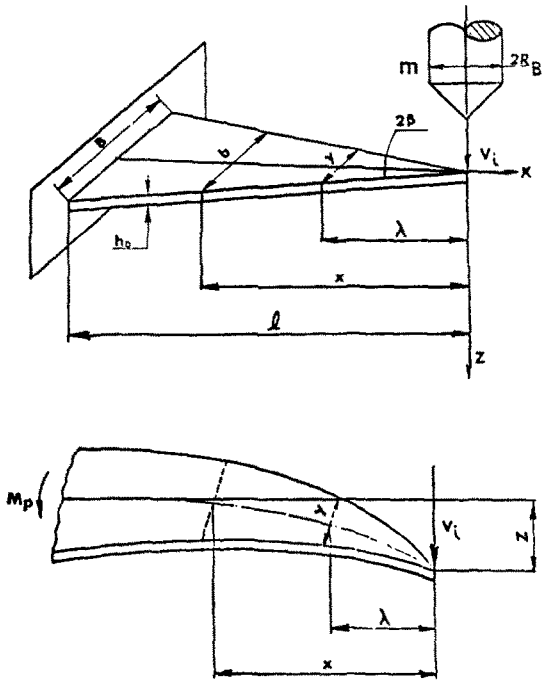

Fig. 9. Petal dimensions and loads.

to that of the projectile divided by the number of petals. This is an idealization and implies a symmetric case.

According to Johnson [10], the velocity of the striking mass, after the hinge reaches the root of the petal, is given by

$$v_1 = \frac{v_i}{1 + \dfrac{\mu}{3m}} \tag{8}$$

where m is the striking mass, and
μ is the mass of the cantilever petal. In the present case (Fig. 9)

$$\mu = \frac{\rho h_0 B l}{2} \tag{9}$$

with ρ as the mass density of the target. If the length of the crack is "a", then B, the width of the root, can be calculated from

$$B = \frac{2\pi a}{n} \tag{10}$$

where the circular geometry of the base has been linearized. If $l = a$, eqn (9) takes the form

$$\mu = \frac{\pi \rho h_0 a^2}{n} . \tag{11}$$

Applying eqn (11) to eqn (8) yields

$$v_1 = \frac{v_i}{1 + k} \tag{12}$$

where

$$k = \frac{\pi \rho h_0 a^2}{3m} \tag{13}$$

and instead of the total mass m, the quantity $\frac{m}{n}$ was substituted in eqn (8).

In the second stage of motion, rigid-body rotation of the petals about their fixed end takes place. The balance of energy for this stage is

$$M_p^* \Theta_s = \Delta W_R + \frac{m}{2n}(v_1^2 - v_f^2) \tag{14}$$

where

$$\Theta_s = \Theta_2 - \Theta_1 \text{ and } M_p^* = Y\frac{Bh_0^2}{4} \tag{15}$$

is the fully plastic moment of the root of the petal obtained by substituting $x = l$ in eqn (6). B is obtained from eqn (10). Further, $\Delta W_R = W_{R_1} - W_{R_2}$ is the change in rotational energy of the petal during the second stage of motion, and v_f is the terminal velocity of the projectile. The rotational energy of the petal at the beginning of the second stage, W_{R_1}, is given by [10]

$$W_{R_1} = \frac{m}{2n} v_i^2 \frac{k}{2(1 + k)^2} \tag{16}$$

while the rotational energy of the petal at the end of the second, W_{R_2}, is

$$W_{R_2} = \tfrac{1}{2} I \omega_f^2 . \tag{17}$$

From Fig. 7

$$\omega_f = \frac{v_n}{a} = \frac{v_f \cos \Theta_2}{a} . \tag{18}$$

For a triangular plate with uniform thickness h_0, the mass moment of inertia I about the base is

$$I = \tfrac{1}{12} B l^3 h_0 \rho = \tfrac{1}{6} \frac{\pi a^4 h_0 \rho}{n} . \tag{19}$$

Substituting eqns (15)–(19) into eqn (14) yields the expression for the terminal velocity v_f as

$$v_f = \sqrt{\frac{\frac{2 + k}{2(1 + k)^2} v_i^2 - \frac{\pi Y a h_0^2 (\Theta_2 - \Theta_1)}{m}}{1 + \frac{\pi a^2 h_0 \rho \cos^2 \Theta_2}{6m}}} . \tag{20}$$

The ballistic limit v_{50} associated with eqn (20) is obtained by setting $v_f = 0$ so that

$$v_{50} = h_0(1 + k)\sqrt{\frac{2\pi Ya(\Theta_2 - \Theta_1)}{m(2 + k)}} . \tag{21}$$

The energy of dishing can be estimated from the results of Ref. [6] where the energy of radial stretching due to stress σ_r and strain $\epsilon_r \simeq \left(\frac{\partial w}{\partial r}\right)^2$ are computed as

$$W_p = \int_V \left(\int \sigma_r \, d\epsilon_r \right) dV \tag{22}$$

integrated over the plate volume V. The work of the circumferential stresses is neglected here. In the present integration, the lower limit is taken as the value of the crack length a and the upper limit is taken as infinity, since the contribution from the outer plate radius will be small. The function $w\langle r\rangle$ is the radial distribution of the final axial plate displacements. In the vicinity of the ballistic limit, this displacement function for 2024-0 aluminum was empirically found to be well represented by [6]

$$w = w_C e^{-br} \tag{23}$$

where w_C is the central deflection and b is a constant. Furthermore, the uniaxial stress-strain curve for this and many other metals can be effectively delineated by a rigid/work-hardening relation of the form

$$\sigma_r = Y + \gamma \epsilon_r \tag{24}$$

where γ is a work-hardening parameter. Substitution of eqns (23) and (24) into eqn (22) yields, with ν as Poisson's ratio

$$\begin{aligned} W_p &= \frac{2\pi h_0}{(1 - \nu + \nu^2)^{1/2}} \int_a^\infty \left[\tfrac{1}{2} Y(b^2)(w_C e^{-br})^2 + \frac{\gamma}{8} (b)^4 (w_C e^{-br})^4 \right] r \, dr \\ &= \frac{2\pi h_0 w_C^2}{(1 - \nu + \nu^2)^{1/2}} \left[\frac{e^{-2ba}}{8} (1 + 2ba) Y + \frac{\gamma}{128} w_C^2 e^{-4ba} (1 + 4ba) \right]. \end{aligned} \tag{25}$$

The magnitude of the ballistic limit including this dishing energy can now be obtained as

$$\begin{aligned} v_{50} &= \frac{2}{m} [W_c + W_p + M_p^*(\Theta_2 - \Theta_1)]^{1/2} \\ &= \frac{2}{m} \left(\frac{2\pi n h_0}{E} [aYF\langle n\rangle]^2 + \frac{2\pi w_C^2 h_0}{(1 - \nu + \nu^2)^{1/2}} \left[\frac{Y(1 + 2ba)}{8} e^{-2ba} \right. \right. \\ &\quad \left. \left. + \frac{\gamma}{128} w_C^2 (1 + 4ba) e^{-4ba} \right] + \frac{2\pi Y a h_0^2}{4} [\Theta_2 - \Theta_1] \right)^{1/2}. \end{aligned} \tag{26}$$

Adjustment of eqn (20) to include the dishing energy term, eqn (25), leads to the relation

$$v_f = \sqrt{\frac{\frac{2 + k}{2(1 + k)^2} v_i^2 - \frac{\pi Y a h_0^2 (\Theta_2 - \Theta_1)}{m} - \frac{2W_p}{m}}{1 + \frac{\pi a^2 h_0 \rho \cos^2 \Theta_2}{6m}}}. \tag{27}$$

THE EFFECT ON TARGET PERFORATION DUE TO THE PRESENCE OF AN INITIAL HOLE, STRUCK NORMALLY AND CENTRALLY BY A CONICALLY-TIPPED PROJECTILE

During the current investigation, a number of experiments were performed involving normal impact of a cylindro-conical projectile at the center of a hole initially drilled in the target plate. The tests were originally designed to find the amount of energy ab-

sorbed in the process of initial plate indentation by the projectile, to be compared with that for the penetration of the intact plate under otherwise identical conditions. The results contradicted expectations. The amount of energy absorbed by the target with an initial hole was larger than for the intact plate. The investigation was then extended to include different diameters of such an initial hole.

The general velocity pattern was found to be as shown in Fig. 10. In this diagram, R_B is the radius of the projectile; R_0 is the radius of an initial hole, $\Delta v = v_i - v_f$ is the velocity drop and v_i, v_f are the initial and final velocities, respectively. An indication of the existence of this phenomenon can be found in Ref. [4] where static punching tests were performed with holes introduced initially. In this work an attempt was made to calculate the amount of plastic work spent in the process of forming a crater due to punch penetration. The analysis was executed for a static case, but using the approach due to Thomson [3]; it can be modified to apply to dynamic punching when the target crater conforms to the projectile shape. Even in other situations, this solution can be used as a first approximation of the plastic work expended during this stage of deformation.

The phenomenon implies a change of the mechanism in the penetration process of the plate within the range of hole radii tested from petalling to extrusion. This bears some similarity to the change of the dominant mechanism from bending to shear found in the perforation of intact plates [10].

When the plate with the drilled hole is first struck by the projectile, hoop stress σ_Θ develops at the circumference of the hole; all other stresses (σ_r, σ_z) are assumed to be zero [10–13]. It will also be assumed that plastic deformation takes place without change in volume and that the stress $\sigma_\Theta = Y$, the yield stress. Constant volume deformation implies thinning of the crater relative to its original thickness of the plate which is neglected in eqns (6)–(20). When the hole grows to a size such that the hoop strain becomes equal to the dynamic tensile fracture strain of the target (which may be different from the static value if the material is strain-rate dependent), the process of petal formation is initiated. This occurs when the distal side crater radius is R_D and the enlarged hole radius is R_E, as shown in Fig. 11. This represents the beginning of the second and third perforation stages here, similar to the process described in the case of crack propagation (stage 1) and plastic bending of petals (stage 2) in the intact plate. Following Refs. [3] and [4], the amount of energy absorbed in the first stage of the deformation is due to plastic deformation and dynamic effects. The first is given by

$$W_p = 2\pi Y h_0 R_E^2 \hat{I} \tag{28}$$

where

$$\hat{I} = \int_{R_0/R_E}^{1} C \ln \left[\sin \alpha + \frac{(1 - \sin \alpha)}{C^{3/2}} \right]^{2/3} dC. \tag{29}$$

The amount of dynamic work in the first stage is evaluated as

$$W_d = \pi \rho h_0 (v_i \tan \alpha)^2 (R_E^2 - R_0^2). \tag{30}$$

Crater radius R_E can be determined from [4]

$$\left(\frac{R_D}{R_E}\right)^{3/2} = 1 - \sin \alpha \left[1 - \left(\frac{R_0}{R_E}\right)^{3/2} \right] \quad \text{or} \quad R_E = \frac{R_D^{3/2} - R_0^{3/2} \sin \alpha^{2/3}}{1 - \sin \alpha}. \tag{31}$$

The total amount of energy absorbed in the first stage is

$$W_1 = W_p + W_d. \tag{32}$$

This relation permits the calculation of the velocity v_{R_D} at the end of the plastic hole

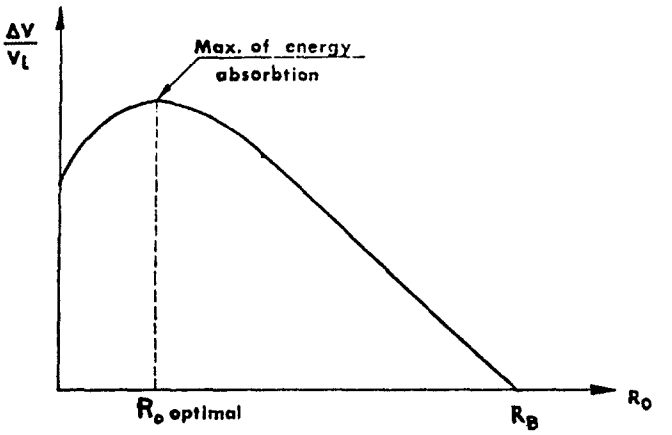

Fig. 10. Qualitative nondimensional velocity drop as a function of initial hole size in a plate for central normal perforation of the hole by a cylindro-conical projectile.

enlargement stage from the energy balance

$$\tfrac{1}{2}m(v_i^2 - v_{RD}^2) = W_1. \tag{33}$$

The analysis of the cracking and additional petal bending stages is much more complicated. The plastic work is determined from the geometry of the crater, shown in the first part of Fig. 11. At the instant depicted there, the star-shaped crack starts to propagate from the tip of the crater outwards and plastic bending of the petals just formed also begins. The model of the petal at the beginning stage of bending is shown in Fig. 12. From this diagram, it may be seen that the petal now has a trapezoidal shape, bent initially through the angle α, the half-cone angle of the projectile, relative to the target plate plane. The same assumptions as stated previously will be employed here for the bending of the petals. Once more, the principal hypothesis is that outward crack propagation precedes the outward movement of the plastic hinge.

According to Ref. [10], the velocity v_h of the projectile at the end of (for this case) the second stage when the plastic hinge arrives at the root of the petal is given by

$$v_h = \frac{v_{RD}}{1 + \dfrac{\rho h' l}{6m_e}(B + 2B_0)}. \tag{34}$$

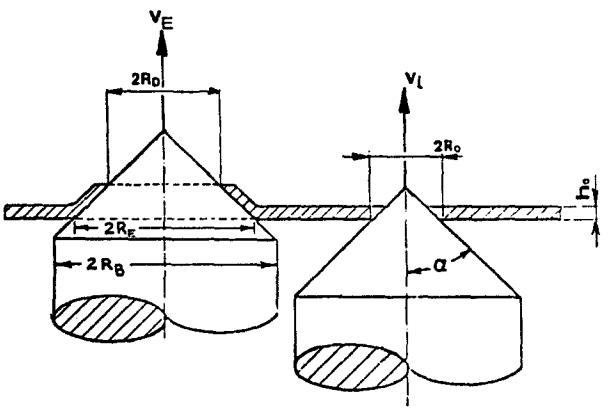

Fig. 11. Plastic hole enlargement.

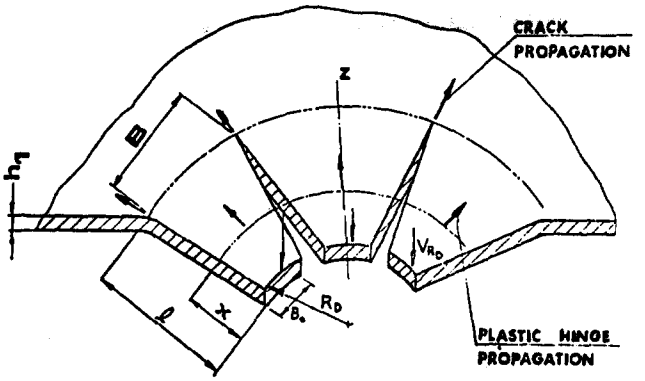

Fig. 12. Plastic hinge and crack propagation in an initially perforated plate struck symmetrically and normally by a cylindro-conical projectile.

In the present case h' is the average thickness of the crater after plastic hole enlargement; $B_0 = \frac{2\pi R_D}{n}$ is the width of the petal at the tip; $B = \frac{2\pi(a + R_D)}{n}$ is the width of the petal at the root, $l = a$ is the length of the radial crack; and $m_e = \frac{m}{n}$ is the equivalent striking mass on one petal. Substituting these parameters into eqn (34) yields

$$v_h = \frac{v_{R_D}}{1 + \frac{\rho h' \pi a}{3m}(a + 3R_D)} = \frac{v_{R_D}}{1 + k_1} \tag{35}$$

where

$$k_1 \equiv \frac{\rho h' \pi a}{3m}(a + 3R_D). \tag{36}$$

At the end of crack propagation and after the hinge is arrested, the petals also rotate through an angle Θ_h, which is small, of the order of 2°, relative to the angle Θ_R occurring in the subsequent rigid rotation of the ensuing stage. The energy balance for this last third stage is given by

$$M_p^* \Theta_R = \Delta W_k + \tfrac{1}{2} m_e (v_h^2 - v_f^2). \tag{37}$$

The energies are given by

$$W_{R_h} = \frac{\rho \pi h' a v_h^2}{12n}(a + 4R_D) \tag{38}$$

which is the kinetic energy of the petals at the end of the second stage and

$$W_{R_3} = \tfrac{1}{2} I \omega_f^2 \tag{39}$$

which is the kinetic energy of the petals at the end of the third stage, and $\Delta W_k = W_{R_h} - W_{R_3}$, where

$$\omega_f = \frac{v_f \cos(\Theta_R + \Theta_h)}{a} \tag{40}$$

and

$$I = \frac{\rho h' B a^3 (a + 4R_D)}{12(a + R_D)} \tag{41}$$

with Θ_R as the angle of rigid rotation during the third stage which, in conjunction with Θ_h, ensures free passage of the projectile, and the plastic moment at the petal root, M_p^*, given by

$$M_p^* = Y\frac{Bh'^2}{4} \tag{42}$$

with

$$B = \frac{2\pi(a + R_D)}{n}.$$

Finally, the terminal velocity can be evaluated in a manner similar to that obtained in the previous section. Substituting eqns (38)–(42) into eqn (37) yields

$$v_f = \sqrt{\frac{\dfrac{1 + k_2}{(1 + k_1)^2}v_{R_D}^2 - \dfrac{Y\pi(R_D + a)h'^2\Theta_R}{m}}{1 + k_2\cos^2(\Theta_h + \Theta_R)}} \tag{43}$$

where

$$k_2 = \frac{\rho\pi h'a(a + 4R_D)}{6m}. \tag{44}$$

In the calculation of the total energy absorbed in the process, the approximation for the energy required to produce plate dishing, eqn 25, has not been included because its form may not apply for impact at the center of a hole in a preperforated target, although this energy is also expected to be predominant near the ballistic limit and is not significant at higher velocities compared to petal bending. The energy represented by eqn (32) absorbed in the crater stage, depends on two parameters: R_0, the initial radius of the hole and R_D, the radius of the enlarged hole at the onset of fracture. The energy involved in the plastic petal bending stage also depends on the parameter R_D. It was found experimentally that for a certain initial magnitude of R_0, the radial cracks disappear completely, which means that R_D, the enlarged radius at the onset of cracking, is equal to the radius of the projectile R_B. In this case, the stage of plastic petal bending does not exist, and the only energy absorption besides dishing is due to cratering. It can be seen from eqns (29)–(33) that if $R_D = R_B = R_0$ the plastic work is zero and the projectile is able to pass through the initial hole without losing any energy. In Ref. [4], the radius R_D is calculated as a function of R_0, but this is applied to static punching. According to this source,

$$R_D = R_0e^{\epsilon_F} \tag{45}$$

where ϵ_F is the fracture strain in a quasi-static tensile test. This relation does not fit the experimental results obtained in the present investigation. For 2024-0 aluminum, the value of ϵ_F was determined as 0.082, and hence $R_D = 1.085R_0$, according to eqn (38). However, results from the perforation tests where no petals were produced exhibited a constant crater diameter $R_D = R < R_B$.

EXPERIMENTAL ARRANGEMENT

Since the energy absorbed in the perforation process was of primary concern of this investigation, the experimental setup was designed to supply this information by measuring the initial and terminal velocities, which permitted the calculation of the initial and terminal kinetic energies. Figure 13 presents a schematic of the test arrangement that consists of a pneumatic ballistic gun with a bore diameter of 12.7 mm, which can

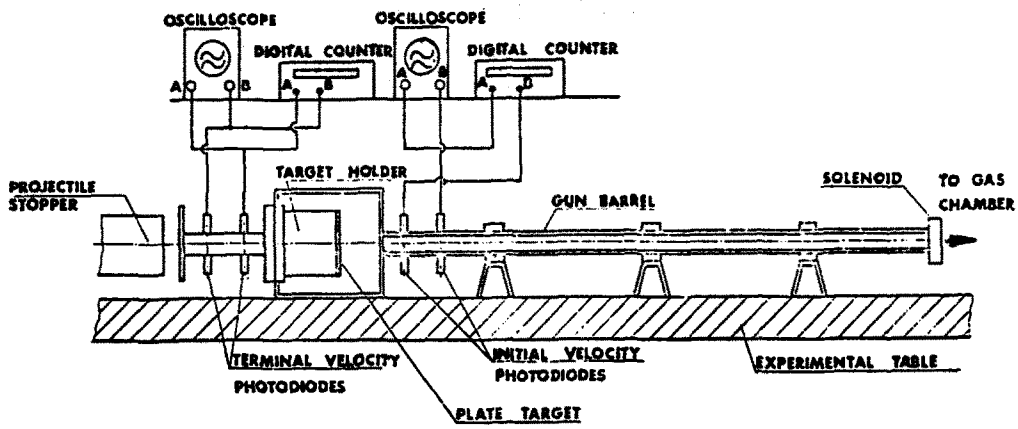

Fig. 13. Schematic of the low-velocity test arrangement.

fire projectiles only in the subordinance velocity range, up to about 300 m/s for spherical steel strikers. The 12.7 mm diameter cylindro-conical projectile was made of heat-treated steel (R_c60) with a 60° conical nose (α = 30°) and a mass of 29.7 g. The initial velocity was measured by their interruption due to projectile passage of two parallel light beams passing through two slits near the end of the barrel and focussed onto two diodes, with the resulting signal recorded simultaneously by an interval counter and an oscilloscope.

The terminal velocity was measured similarly with a pair of photodiodes placed behind the target. The target consisted of 139.7 mm diameter 2024-0 aluminum plates with two different thicknesses, 1.27 and 3.175 mm.

The experiments in the range from 300–600 m/s were performed at the Naval Weapons Center, China Lake, California, by means of a powder gun. The initial velocity was also measured in identical fashion with photodiodes. The terminal velocity was determined from pictures taken by a six-frame KFC-600 Kerr cell camera, which used a focusing shadowgraph back-lighting scheme. The arrangement and the experimental procedure are described in Ref. [11].

RESULTS AND DISCUSSION

Calculations have been performed for the perforation of an intact 2024-0 aluminum plate of 3.13 mm thickness by a 29.5 g cylindro-conical steel projectile with a 30° half-cone angle. The crack length is assumed as 10.16 mm, from which the angle Θ_R generated during petal rotation is calculated as 1.134 rad based on the geometry of Fig. 7, with Θ_h taken as 2°. The quasistatic stress-strain curve of the target material is shown in Fig. 14. This diagram exhibits an actual quasistatic yield stress of 88.3 MPa, but also indicates that the best approximation of the material as a rigid/linear work-hardening solid is given by the expression

$$\sigma = \sigma_r = Y + \gamma\epsilon = Y + \alpha\epsilon_r = 165.5 + 836.4\epsilon_r \text{ MPa}. \tag{46}$$

In the theoretical predictions, six cracks, a static yield stress Y = 165.5 MPa and a Young's Modulus E = 68.956 GPa have been utilized for the evaluation of W_c = 2.76 J which is small compared to W_p = 35.6 J and $M_p^*\Theta_r$ = 30.19 J. Equations (26) and (27) have been evaluated and plotted in Fig. 15 and are in excellent agreement with corresponding experimental results except near the ballistic limit. Here, eqn (26) leads to a value of v_{50} = 70 m/s (compared to a value of 46.3 m/s predicted by eqn (21) with Y = 165.5 MPa); the experimental results seem to indicate a ballistic limit of about 90 m/s. The discrepancy is attributed to the fact that some energies have been left out of the energy balance, such as the work performed by the circumferential stresses in plate dishing, as well as to some experimental uncertainties. The difference becomes unimportant at higher velocities where the dishing energy is but a small fraction of the initial

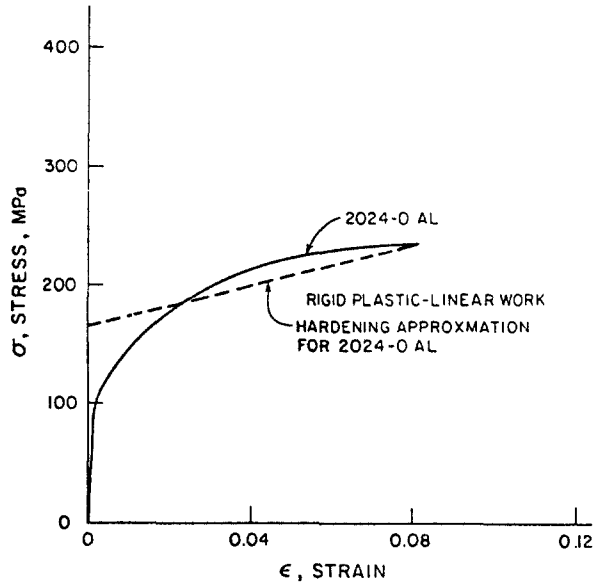

Fig. 14. Quasi-static stress-strain curve of 2024-0 aluminum.

energy, so that differences in the actual plate profile and that ascertained near the ballistic limit will have little influence.

For comparative purposes, the energy absorbed in petal bending determined from the plastic hinge analysis described has been calculated for the velocity range from 90 to 900 m/s using the static value of the yield stress $Y = 88.3$ MPa. The results for two thicknesses of the 2024-0 aluminum plate, $h_0 = 1.27$ and 3.175 mm, have been compared with the theories of Ref. [3] and [12] in Fig. 16. Reference [3] underestimates the absorbed plastic energy in the low-velocity range, a situation that would be further aggravated if that theory were to take into account the dishing of the target that is significant at these speeds. The theory of Ref. [12] is not able to accurately predict the energy absorbed in the penetration process at low velocities since, being a pure momentum balance, it does not consider any parameters related to the strength of the target. In the ordnance range, above 600 m/s, the Thomson and plastic hinge theories are in good agreement, while the values obtained by Paul and Zaid are higher. A change of the value of the yield stress so as to represent more nearly a perfectly-plastic material,

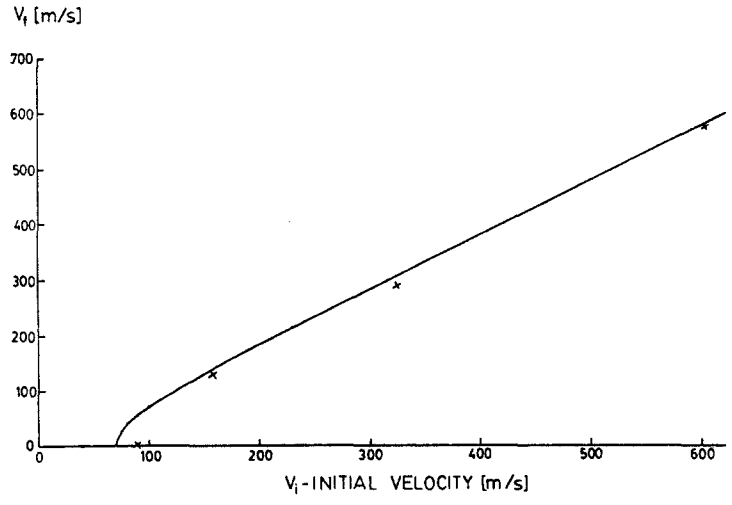

Fig. 15. Comparison of predicted and measured terminal velocity in the normal impact of a 12.7 mm diameter cylindro-conical projectile with a mass of 29.5 g against a 3.175 mm thick intact 2024-0 aluminum target.

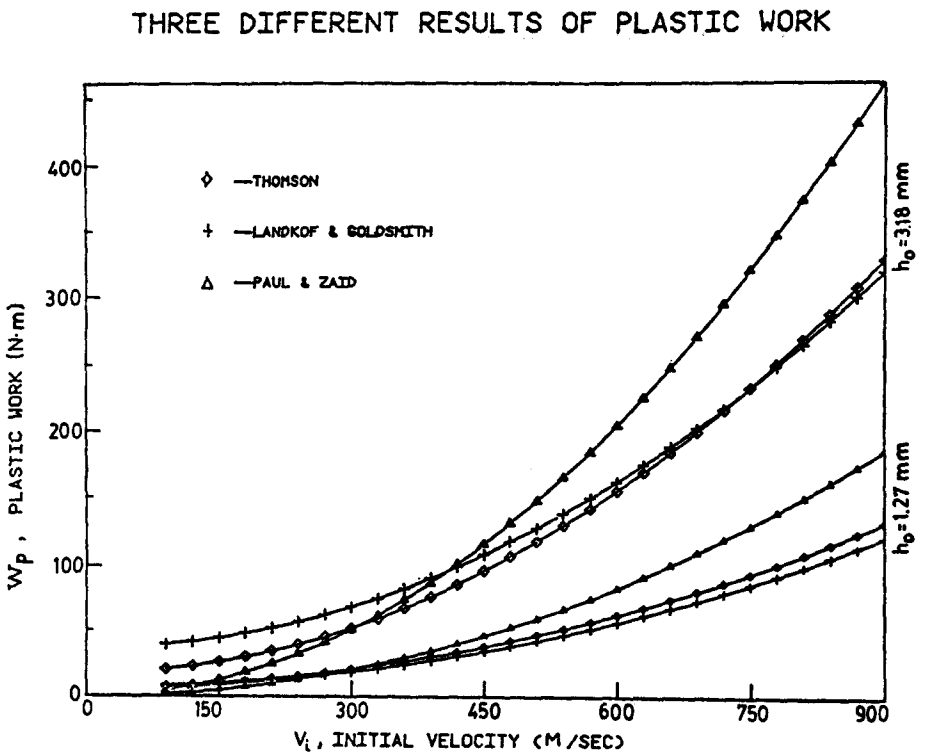

Fig. 16. Energy of petal bending determined by three theories for the normal penetration of a 29.5 g steel projectile with a diameter of 12.7 mm and a half-cone tip angle of 30° against two thicknesses of 2024-0 aluminum.

say to 200 MPa, will change the amount of energy absorbed in petal bending proportionally, but will not influence the relative agreement of the curves in the diagram.

In the solution of the plastic hinge model for petal bending, it was assumed that the thickness of the petals remained unchanged and, further, that no significant circumferential stretching of the petals occurred. This last assumption has been verified by Paul and Zaid [12] by rolling back the petals to their initial position.

A change in the frontal projectile configuration to a blunter shape will eventually transform the perforation process from petalling to plugging. Johnson [4] performed experiments showing that plugging will occur for half-cone angles greater than 45° in static perforation of 3.175 mm aluminum plates by a 12.7 mm diameter punch. A similar effect was investigated here in a series of tests in which the tip of the cone of the projectile was ground to various hemispherical radii and the resultant striker was fired normally at this 3.175 mm thick 2024-0 aluminum plate (Brinell Hardness about 50) at a nominal speed of 150 m/s. The results are presented in Table 1 and indicate a slight increase in the velocity drop $\Delta v = v_i - v_f$ when the tip is changed from the sharp cone to a hemisphere with a radius about 40% that of the projectile machined onto the cone end; further increases in this radius do not produce any corresponding increase in the velocity drop. However, closer to the ballistic limit, this change in geometry may very well have an influence for tip radii up to that of the projectile.

In a separate investigation, it was found that a Teflon coating of the cylindro-conical steel projectiles produced no difference in the residual velocity when perforating intact 3.175 mm 2024-0 aluminum plates at normal incidence with a speed of either 125 or 150 m/s. Substantially greater penetrability has been recently claimed for lead strikers coated with this material.

The energy analysis of the target perforation process for the case of central normal projectile impact on a predrilled hole is hampered by (a) the need for a dynamic relation between R_D, the enlarged radius at the onset of cracking, and the initial hole radius R_0 and (b) the determination of a suitable relation for the energy of dishing for the present case. An investigation carried out at an initial velocity of about 150 m/s using

Table 1. Penetration data for cylindro-conical projectiles with a 60° total cone angle striking 2024-0 aluminum plates of 3.175 mm thickness normally at a nominal speed of 150 m/s

Projectile No.	Mass, g	Nominal Diameter mm	Nominal Length, mm	Tip Radius, mm	Initial Velocity v_i, m/s	Final Velocity v_f, m/s	Velocity Drop, $\Delta v/v_i$, %
1	29.5	12.45	38.1	0	154.1	124.0	19.7
					157.8	127.4	19.2
2	27.8	12.32	35.55	1.27	153.7	118.3	23.0
3	27.8	12.32	35.55	2.54	151.4	109.6	27.6
4	29.6	12.32	35.55	3.81	151.3	112.7	25.7
5	30.7	12.32	35.55	5.08	150.6	--	--
6	28.7	12.32	33.02	6.35	151.6	114.5	24.5

Projectiles 1 and 2 generated only petals, 3 and 4 produced petals and plugs, and 5 and 6 resulted in a plug and small cracks in the target.

12.5 mm diameter, 29.5 g cylindro-conical steel projectiles with a 30° half-cone angle orthogonally striking the center of holes of various radii drilled into 3.175 mm thick 2024-0 aluminum targets, produced the variation in petal length shown in Fig. 17. For the intact plate, the average petal length was found to be $a = 11.4$ mm, which decreased to zero at a value of $R_0/R_B = \frac{2}{3}$, or $R_0 = 4.15$ mm. Beyond this point, only hole enlargement occurs, and the process is similar to that described in Ref. [3]. Furthermore, the energy of plate dishing is expected to be substantially less than when cracks are formed, and can most likely be neglected even relatively close to the ballistic limit. Under these circumstances, the terminal velocity given by eqn (43) is replaced by the expression

$$v_f = \frac{2}{m}\left[v_i^2 - 2\pi Y h_0 R_B^2 \hat{I}_1 - \pi\rho h_0 (v_i \tan\alpha)^2 (R_B^2 - R_0^2)\right]^{1/2} \tag{47}$$

with

$$\hat{I}_1 = \int_{R_0/R_B}^{1} C \ln\left[\sin\alpha + \frac{1 - \sin\alpha}{C^{3/2}}\right]^{2/3} dC. \tag{48}$$

These relations are obtained from an energy balance on the projectile using only eqns (28) and (29) with $R_E = R_B$.

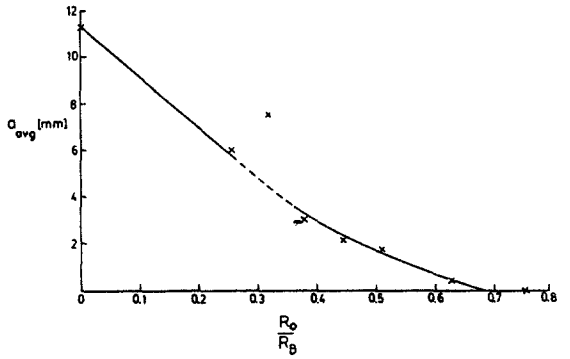

Fig. 17. Petal length as a function of initial hole radius for the normal penetration of 3.175 mm thick 2024-0 aluminum plates by a 29.5 g hard-steel cylindro-conical projectile of 12.5 mm diameter fired against the hole center at a velocity of 150 m/s.

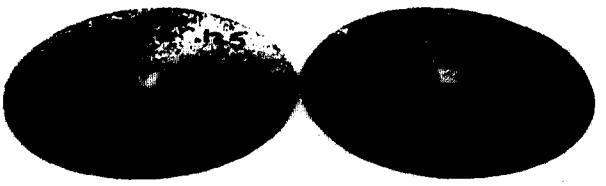

Fig. 18. Photograph of terminal configuration of an initially intact and preperforated 3.275 mm thick 2024-0 aluminum target with an original hole diameter of 3.175 mm by a cylindro-conical projectile with a mass of 29.5 g, a diameter of 12.65 mm and a half-cone angle of 30° at a velocity of about 130 m/s. Left: initially perforated target; right: initially intact target.

At the critical value of $R_0 = 4.15$ mm, the measured base radius $R_D = 6.172$ mm, leading to a critical circumferential tensile strain value of $\epsilon = 0.397$ according to eqn (45) beyond which cracking ensues. Figures 18 and 19 depict the metamorphosis from petalling to pure hole enlargement of the targets.

Equation (47) yields a value of $\Delta v/v_i = 1.08\%$ for an initial velocity of 157.4 m/s and a yield stress $Y = 165.4$ MPa; it gives the proper result $v_i = v_f$ when $R_B = R_0$. In all likelihood, both the critical value of R_0 and the crack length variation below this point are functions of both initial velocity and thickness of the soft aluminum target plate, as well as the projectile cone angle. Thus, the present data do not permit a generalization that might apply to different impact conditions, nor to other target materials.

In the domain of crack propagation, the results of eqn (43) have been portrayed in Fig. 20 for two initial velocities and assumed crack lengths and a value of $Y = 88.3$ MPa for the 3.175 mm thick 2024-0 aluminum target. The relationship between crack length a and R_0 is taken from Fig. 17 as a (mm) $\cong 11.43 - 2.65\,R_0$ for $R_0 < 4.23$ mm; the relation between R_D and R_0 was taken as $R_D = 1.455R_0$ from eqn (45) and corresponding measurements. Since the latter equation was found not to be appropriate, in view of the neglect of plate dishing energy and failure to include the known work-hardening characteristics, the results shown can only be regarded as qualitative. For this reason, an improvement in the value of k_2, given as $k_2 = \rho\pi h(a - R_D)(a + 3R_D)/6m$

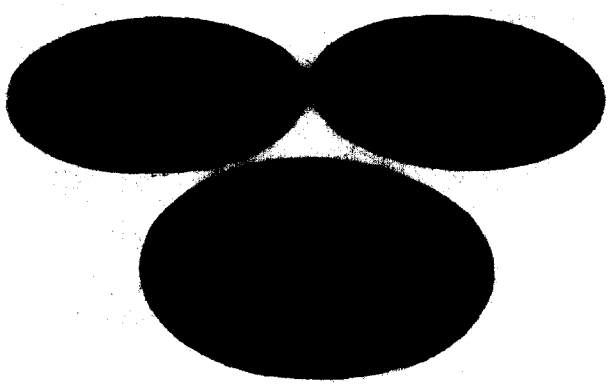

Fig. 19. Photograph of the terminal configurations of three predrilled aluminum targets perforated as in the case of Fig. 18. Left: initial hole diameter = 4.76 mm; center: initial hole diameter = 6.35 mm; right: initial hole diameter = 9.53 mm.

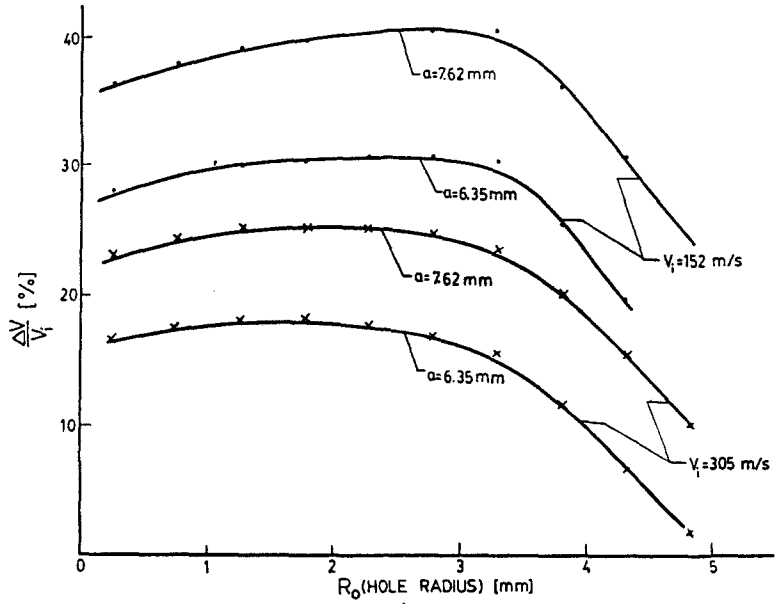

Fig. 20. Calculated results for the velocity drop as a function of hole size for the normal perforation of a predrilled 3.175 mm thick 2024-0 aluminum plate by a 29.5 g hard-steel projectile of 12.45 mm diameter with a 30° half-cone angle for initial velocities of 152 and 305 m/s and two crack lengths.

as well as the addition of an angle β

$$\beta = \sin^{-1}\left[\frac{(R_D - R_0)\cos\alpha}{a(1 - \sin\alpha)}\right]$$

in the cosine term of the denominator of eqn (43) were not carried out. Nevertheless, Fig. 20 depicts the general trend of the experimentally observed behavior, shown in Figure 21, for the non-dimensional velocity drop due to perforation as a function of

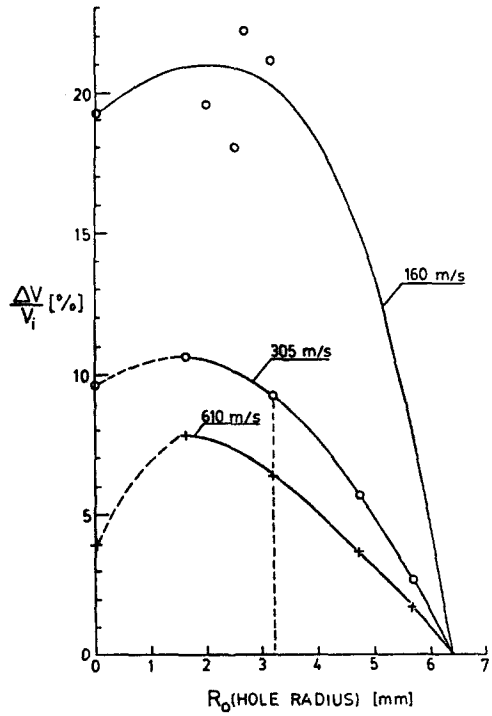

Fig. 21. Experimental nondimensional velocity drop as a function of hole size.

initial hole size, even though the choice of this variable further exaggerates the discrepancy. In both cases, more energy is required to perforate the target at a value of about $0.25R_0$ than for any other hole size or the intact plate for both of the initial velocities investigated, respectively. A serious problem in attempting to secure data between the intact plate and the case of a 3.175 mm diameter hole involved the difficulty of achieving a concentric impact and resultant significant aberrations in terminal velocity (decreases) when the desired point is not struck by the projectile.

Thus, both analytical considerations and test results indicate the existence of an optimum initial hole size for energy absorption at a definite initial velocity. This optimum is probably also a function of such parameters as thickness, material properties and the cone angle of the striker. The relationship between these parameters and the peak energy absorption should be studied further.

CONCLUSION AND RECOMMENDATIONS

The approach of obtaining the energy absorbed in the perforation process of thin, metallic targets by cylindro-conical projectiles used in this paper is based on plastic hinge theory for a study of petal bending. The theory also takes into account dynamic effects and the energy needed for extension of radial cracks which was found to be small relative to the work of plastic bending of petals. The addition of a dishing term then provides a complete model for at least approximately predicting the energy absorption in target plates failing by petalling.

The influence of an existing hole in the target on the perforation process was also investigated. It was found experimentally that, for a given material and geometric impact configuration, an optimum size of hole exists for which energy absorption in perforation is maximal, and that this peak may be a function of initial velocity. This type of behavior was confirmed by a theoretical development that used the same concept of plastic hinges and the change in geometry introduced by the existing hole. The initial process in this case includes plastic hole enlargement until the circumferential fracture strain is attained. This stage is followed by radial crack propagation and plastic petal bending. The size of an initial hole has an influence on the ratio of absorbed energies in these two different processes. If the diameter of the initial hole is large enough, petalling will not occur at all, since the circumferential strain obtained in the plastic hole enlargement remains below the fracture strain throughout the entire process, and the projectile perforates the target only by cratering.

Further studies are suggested that would

a) more accurately describe the energy absorbed in dishing;
b) establish experimentally the dynamic relationship between the cone angle of the projectile and petalling or plugging processes;
c) determine the dynamic relationship between the radius of an enlarged hole at the outset of cracking (R_D) and the initial radius of a hole (R_0);
d) include experiments with initial holes smaller than 3.175 mm dia. in order to find the exact optimal hole size for maximum energy absorption without extrapolation; and
e) include large deformations (and also possible large strains) in the theory similar to that performed by Ting [14].

Acknowledgment—The authors gratefully acknowledge the substantial assistance of Mr. Dan Chen in the conduct of this investigation. This work was sponsored by the Army Office of Research under Contract DAAG 29-80-K-0052.

REFERENCES

1. H. Bethe, *An Attempt at a Theory of Armor Penetration*, Frankford Arsenal (1941).
2. G. I. Taylor, *Quart. J. Mech. Appl. Math.* 1, 103–124 (1948).
3. W. T. Thomson, *J. Appl. Physics* 26, 80–83 (1951).
4. W. Johnson, et al., *J. Strain Analysis* 8:3, 228–241 (1973).
5. J. M. Krafft, *J. Appl. Physics* 26, 1248–53 (1955).
6. C. A. Calder and W. Goldsmith, *Int. J. Solids Structures* 7, 863–881 (1971).
7. G. R. Irwin, *Fracture Dynamics in Fracturing of Metals*. Am. Soc. of Metals, Cleveland, 1948.

8. R. A. Westmann, *J. Math Physics* **43:3,** 191–198 (1964).
9. E. W. Parkes, *Proc. R. Soc.*, Series A, **228,** 462–476 (1955).
10. W. Johnson, *Impact Strength of Materials*. E. Arnold, London, 1972.
11. W. Goldsmith and S. A. Finnegan, *Int. J. Mech. Sci.* **13,** 843–866 (1971).
12. M. Zaid and B. Paul, *J. Franklin Inst.* **264,** 117–126 (1957).
13. M. Zaid and B. Paul, *J. Franklin Inst.* **265,** 317–335 (1958).
14. T. C. T. Ting, *J. Appl. Mech.* **32,** 295–302 (1965).